Cannabidiol-loaded microspheres incorporated into osteoconductive scaffold enhance mesenchymal stem cell recruitment and regeneration of critical-sized bone defects

Amir Kamali[a,b], Ahmad Oryan[a,*,1], Samaneh Hosseini[b], Mohammad Hossein Ghanian[c], Maryam Alizadeh[c], Mohamadreza Baghaban Eslaminejad[b,**,2], Hossein Baharvand[b]

[a] Department of Pathology, School of Veterinary Medicine, Shiraz University, Shiraz, Iran
[b] Department of Stem Cells and Developmental Biology, Cell Science Research Center, Royan Institute for Stem Cell Biology and Technology, ACECR, Tehran, Iran
[c] Department of Cell Engineering, Cell Science Research Center, Royan Institute for Stem Cell Biology and Technology, ACECR, Tehran, Iran

ARTICLE INFO

ABSTRACT

Recruitment of mesenchymal stem cells (MSCs) to an injury site and their differentiation into the desired cell lineage are implicated in deficient bone regeneration. To date, there is no ideal structure that provides these conditions for bone regeneration. In the current study, we aim to develop a novel scaffold that induces MSC migration towards the defect site, followed by their differentiation into an osteogenic lineage. We have fabricated a gelatin/nano-hydroxyapatite (G/nHAp) scaffold that delivered cannabidiol (CBD)-loaded poly (lactic-co-glycolic acid) (PLGA) microspheres to critical size radial bone defects in a rat model. The fabricated scaffolds were characterized by X-ray diffraction (XRD) and scanning electron microscopy (SEM), and then analyzed for porosity and degradation rate. The release profile of CBD from the PLGA microsphere and CBD-PLGA-G/nHAp scaffold was analyzed by fluorescence spectroscopy. We performed an in vitro assessment of the effects of CBD on cellular behaviors of viability and osteogenic differentiation. Radiological evaluation, histomorphometry, and immunohistochemistry (IHC) analysis of all defects in the scaffold and control groups were conducted following transplantation into the radial bone defects. An in vitro migration assay showed that CBD considerably increased MSCs migration. qRT-PCR results showed upregulated expression of osteogenic markers in the presence of CBD. Histological and immunohistochemical findings confirmed new bone formation and reconstruction of the defect at 4 and 12 week post-surgery (WPS) in the CBD-PLGA-G/nHAp group. Immunofluorescent analysis revealed enhanced migration of MSCs into the defect areas in the CBD-PLGA-G/nHAp group in vivo. Based on the results of the current study, we concluded that CBD improved bone healing and showed a critical role for MSC migration in the bone regeneration process.

1. Introduction

Bone healing is a complicated biological process that consists of an initial inflammatory response followed by recruitment and differentiation of mesenchymal stem cells (MSCs) [1,2]. Incomplete regeneration of critical-sized bone defects are principally related to the inadequate migration of MSCs into the defect site and inability of the migrated MSCs to fully differentiate into osteogenic precursor cells [3]. Numerous bone substitutes have been developed that combine exogenous cells with biomaterials to improve the healing process of large-sized defects [4,5].

MSCs have the capability to differentiate into an osteoblastic cell lineage. They release cytokines which modulate the inflammatory response and induce production of various growth factors [3]. However, limitations to the in vivo use of exogenous MSCs for regeneration of critical-sized bone defects include poor proliferation and osteogenic diffrentation [6]. Hence, development of a novel scaffold that can recruit MSCs to an injury site and allow them to differentiate into
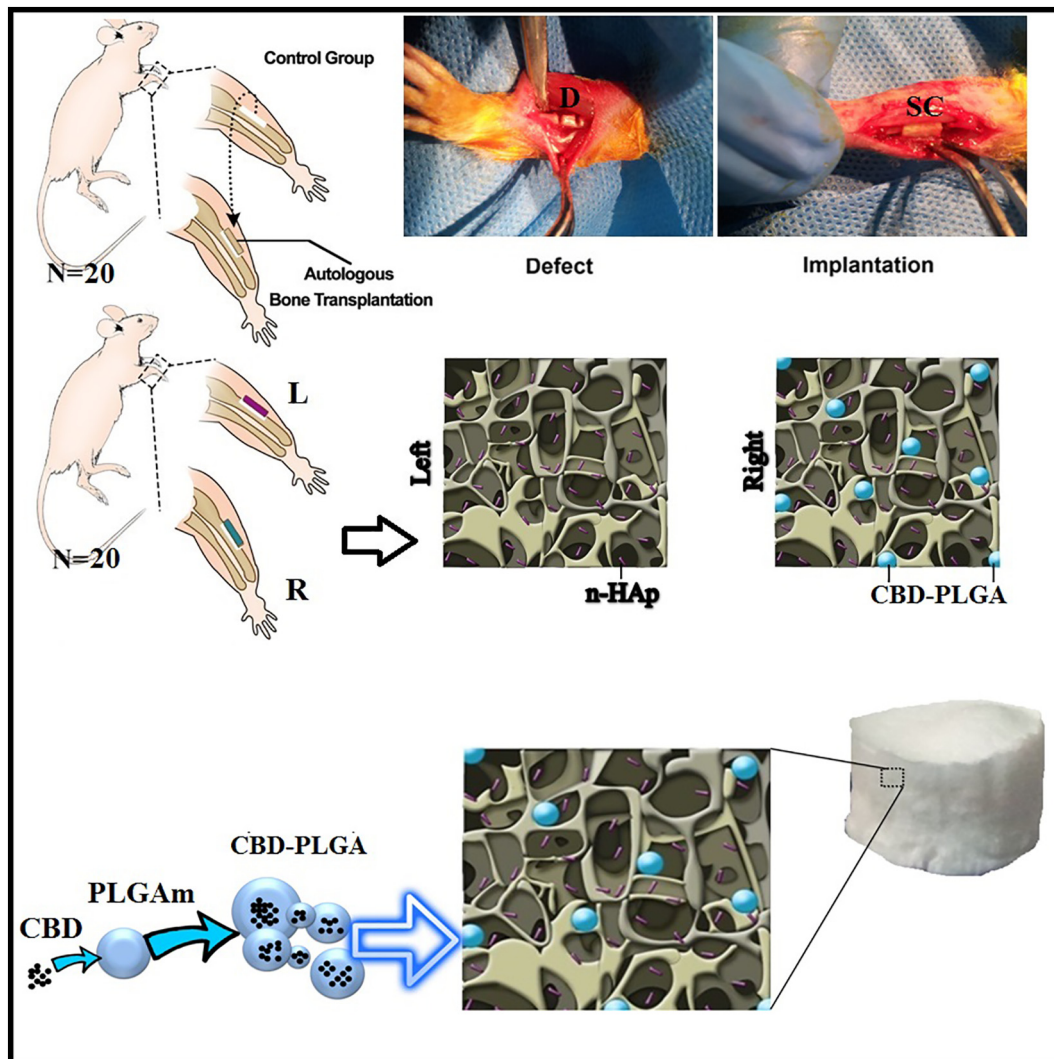
Fig. 1. Schematic representation of various groups and subsequent treatment protocols; Sc: scaffold, Se: segmental defect, nHAp: nano-hydroxyapatite, CBD: cannabidiol, PLGA: poly (lactic-*co*-glycolic acid).

osteogenic lineages would be an alternative strategy to exogenous MSCs.

Stromal cell-derived factor-1 (SDF-1) is a chemokine protein encoded by the C-X-C motif chemokine ligand 12 (*CXCL12*) gene. Binding of SDF-1 to its main receptor [C-X-C chemokine receptor type 4 (CXCR4)] triggers migration of MSCs and other progenitor cells into the injury site [7]. SDF-1 has been combined with scaffolds or loaded into microspheres to facilitate migration of MSCs into large bone defects [8–10]. Because SDF-1 is susceptible to degradation, denaturation, and inactivation [11,12], bioactive molecules have been introduced as alternatives [13]. Cannabidiol (CBD) is a bioactive molecule that can increase in vitro MSC migration [14]. CBD is one of the known 113 active cannabinoid compounds identified in cannabis, a phytocannabinoid [15]. The pharmacological effects of cannabinoid compounds include analgesia, muscle relaxation, immunosuppression, anti-inflammatory, anti-allergic, neuroprotection, and antineoplastic effects [16]. Numerous clinical trials have been conducted with cannabinoid compounds as treatment for Dravet syndrome and epilepsy [17,18]. According to research, the cannabinoid ligands efficiently improved ovariectomy-induced bone loss and enhanced fracture healing [19,20]. CBD receptors (CB1 and CB2) are important mediators of the tissue healing process [21,22]. Most of the cannabinoid impacts on the bone and skeletal system are attributed to these receptors and their ligands. In particular, CB2 signaling has a regulatory effect on several pro-

osteogenic processes [23]. Schmuhl et al. have shown that CBD enhanced migration of MSCs via activation of P42/44 MAPK, and subsequently induced MSC differentiation into an osteoblastic lineage under in vitro conditions [14]. Systemic delivery via an intraperitoneal injection of CBD on bone healing was examined in a rat fracture model [19]. In this study, the researchers observed that CBD resulted in fracture healing and improved biomechanical properties of the fracture callus by enhanced *PLOD1* gene expression, which encodes an enzyme involved in collagen crosslinking [19].

In the current study, we fabricated a novel scaffold to recruit MSCs into large bone defects by using CBD-loaded microspheres incorporated into an osteoconductive scaffold. Next, we analyzed the short- and long-term osteogenic activities of CBD under in vitro and in vivo conditions by real-time PCR, histopathology, histomorphometry, immunohistochemistry (IHC), and micro-computed tomography (micro-CT) scan.

2. Materials and methods

2.1. Materials

CBD was obtained from Tocris Company (Tocris, Bio-Techne Corporation, USA). Poly (lactic-*co*-glycolic acid) (PLGA, 50:50, Resomer® RG 503H, inherent viscosity: 0.32–0.44 dl/g), polyvinyl
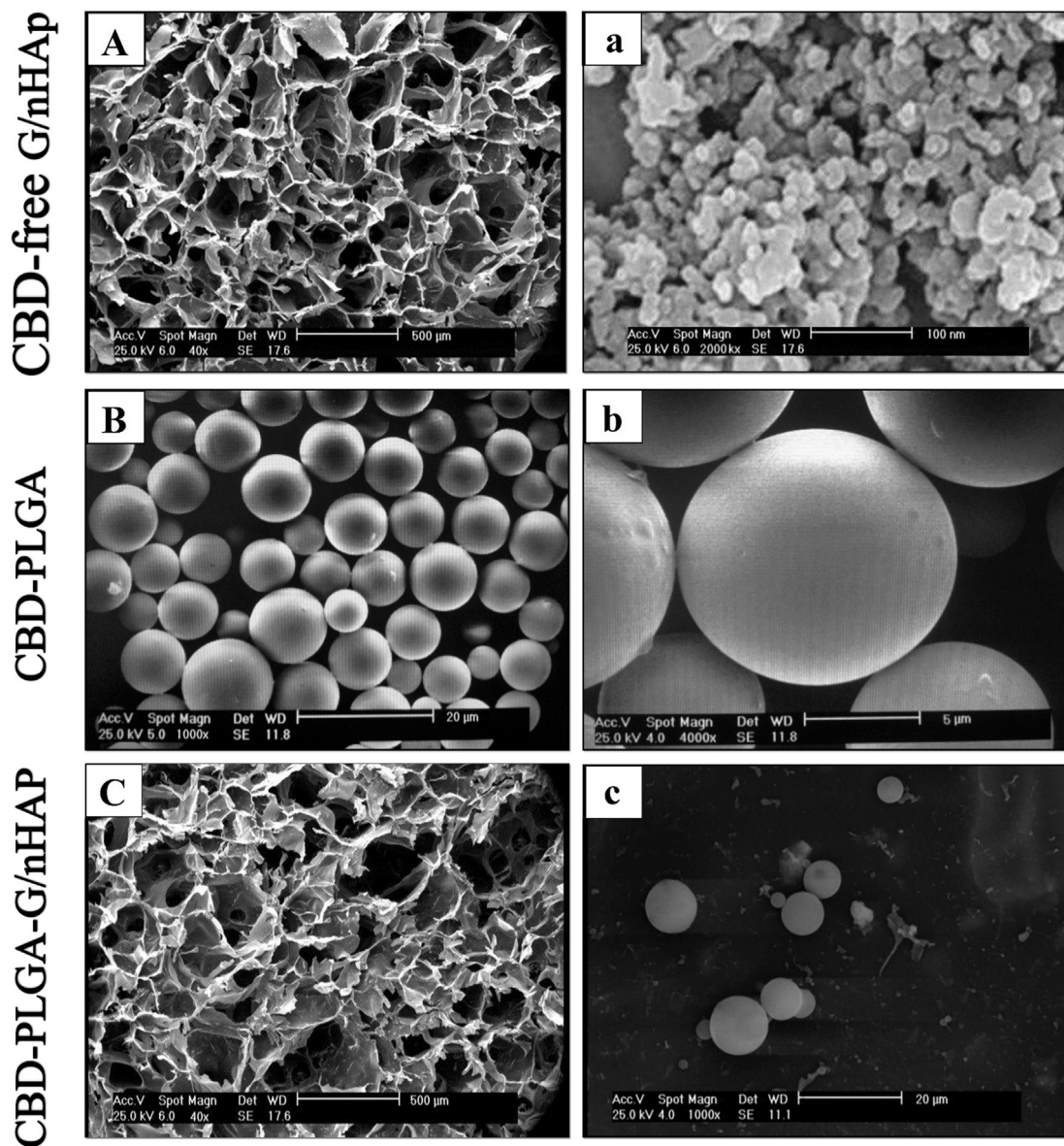
Fig. 2. SEM micrographs of the CBD-free G/nHAp (A, a), CBD-PLGA microspheres (B, b) and CBD-PLGA-G/nHAp (C, c) scaffolds prepared by the freeze-drying method. The G/nHAp scaffold show a homogeneous porous structure.

alcohol (PVA, mw 30,000–70,000), Tween 20, and dichloromethane (DCM) were purchased from Sigma-Aldrich (USA). Gelatin (Gel-bovine skin, type B, isoelectric point ~5) was purchased from Sigma-Aldrich (St. Louis, MO, USA). N-hydroxysuccinimide (NHS, 97%) was obtained from the Aldrich Chemical (Milwaukee, WI, USA). 1-Ethyl-3-(3-di-methylaminopropyl) carbodiimide hydrochloride (EDC) was purchased from Sigma-Aldrich (Milano, Italy).

2.2. Methods

2.2.1. Scaffold preparation

In order to fabricate the G/nHAp scaffold, we added 0.1 g nHAp to 20 ml of 5% w/v gelatin solution. The solution was stirred for 12 h at 37 °C. The resultant gel was maintained at −20 °C for 24 h, and then freeze-dried. EDC and NHS (in a 2:1 ratio) were dissolved in acetone [90% v/v in distilled water (DW)] and then added the freeze-dried gel to chemically crosslink the scaffolds. The scaffolds were washed in DW, freeze-dried, and sterilized in 70% ethanol and UV light for subsequent experiments.

2.2.2. Fabrication of the CBD-PLGA microspheres

We used a single emulsion (O/W) solvent evaporation method to prepare PLGA microspheres that contained CBD. Briefly, 30 mg of polymer and 3 mg of CBD were dissolved in 2 ml of DCM. This oil phase was added to 5 ml of an aqueous solution of 1% w/v PVA that contained Tween 20, and homogenized for 3 min at 7000 rpm (Heidolph Silent Crusher M, Germany) in an ice bath. The emulsion was immediately added to 100 ml of an aqueous solution of PVA (0.1% *w/v*). The extraction step was followed by stirring for 3 h at 300 rpm at room temperature to allow the organic solvent to evaporate and for solidification of the microspheres. The microspheres were collected by centrifugation for 20 min at 9000 rpm and washed 3 times with DW to remove the residual surfactants. The microspheres were frozen at −20 °C, lyophilized, and stored at −20 °C until use.

2.2.3. Fabrication of the blank and CBD-PLGA microsphere incorporated scaffolds

The CBD-PLGA microsphere incorporated scaffold (CBD-PLGA-G/nHAp) was prepared using a previously described post-seeding technique [24]. Briefly, 1 mg of CBD-PLGA was suspended in 1 ml DW. We
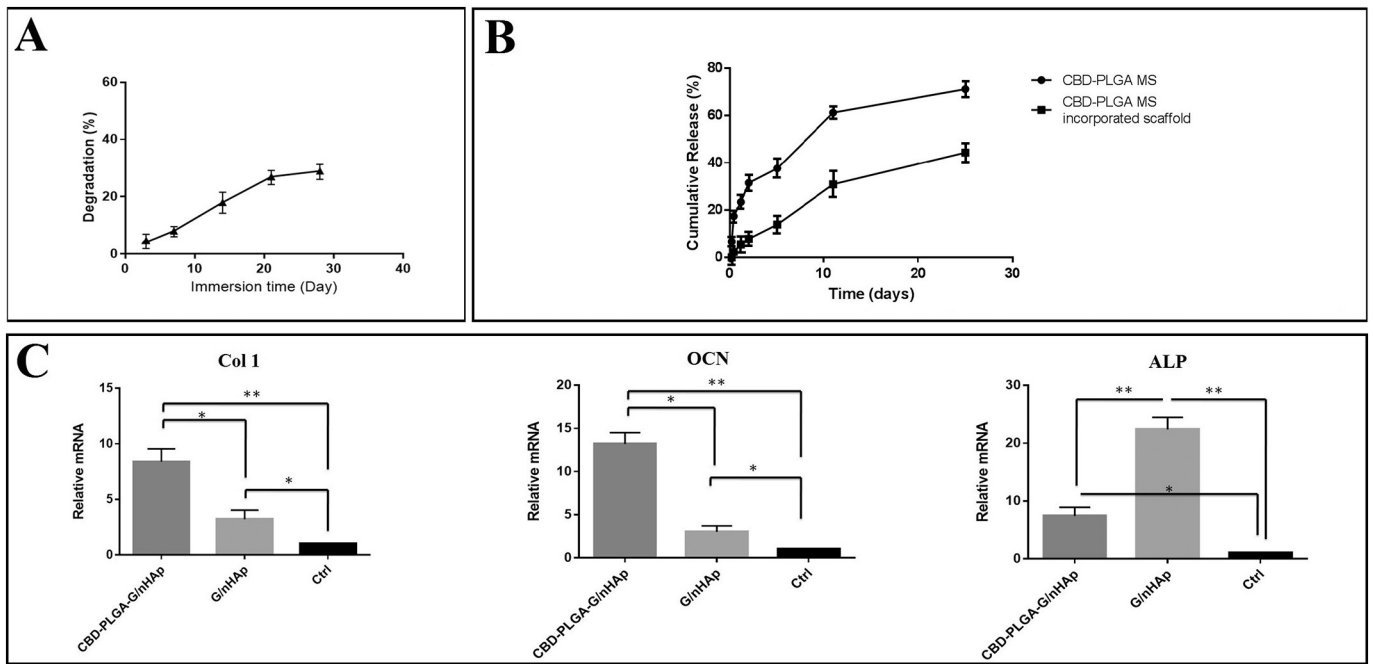
Fig. 3. Characterization of bioscaffolds; A) in vitro release of CBD from PLGA microsphere and CBD-PLGA-G/nHAp scaffold in PBS during 25 days. B) Biodegradability of G/nHAp scaffold. C) Effects of the scaffolds on mRNA expression of the OCN, ALP, and ColI genes on day 21.
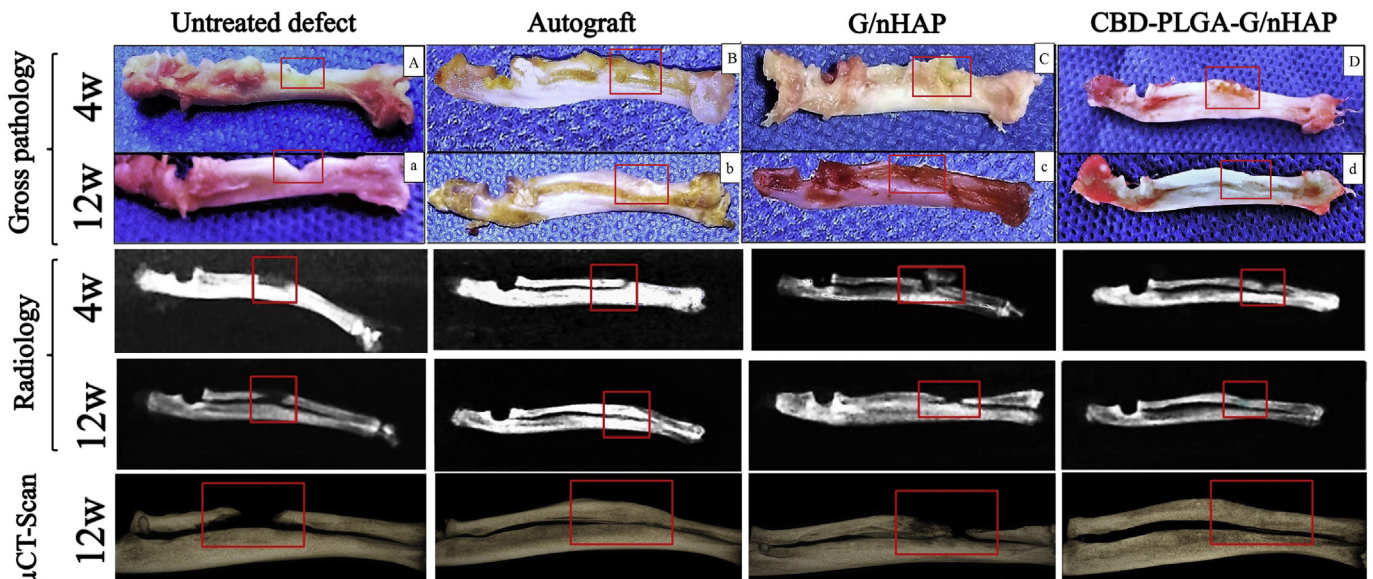

Fig. 4. Macroscopic and diagnostic imaging (X-ray and Micro CT) of the radial bone defects 4 and 12 week post-surgery (micro-CT scan data obtained only at 12 week post-surgery).

Table 1
Macroscopic scores of the healed defects at 12 weeks.

Type of evaluation	Untreated defect (1) Median (min-max)	Autograft (2) Median (min-max)	G/nHAp (3) Median (min-max)	CBD-PLGA-G/nHAp (4) Median (min-max)	P^{a}
Macroscopic	1 (0-1)	3 (3-3)	1 (1-1)	2 (2-3)	0.003

G: gelatin, nHAp: nano hydroxyl apatite, CBD: cannabidiol, PLGA: poly (lactic-*co*-glycolic acid) microsphere.

Complete union (+3 score), presence of cartilage (+2 score), presence of soft tissue (+1 score), nonunion (0 score).

$P < 0.01$ (1 vs. 2 and 4), (3 vs. 2); $P < 0.05$ (3 vs. 4).

[a] Kruskal–Wallis non-parametric ANOVA.

Table 2
Results obtained from radiographical evaluations of the regenerated defects at 4 and 12 weeks.

Post-operative weeks	Untreated defect (1) Median (min-max)	Autograft (2) Median (min-max)	G/nHAp (3) Median (min-max)	CBD-PLGA-G/nHAp (4) Median (min-max)	P^a
4	0 (0-0)	4 (5-6)[b]	2 (1-2)[d]	3 (3-5)[f]	0.002
12	1 (0-1)	8 (7-9)[c]	4 (3-5)[e]	n (6-7)[g]	0.003

G: gelatin, nHAp: nano hydroxyl apatite, CBD: cannabidiol, PLGA: poly (lactic-*co*-glycolic acid) microsphere.
[b,c]$P < 0.01$ (2 vs. 1) and [b,c]$P < 0.05$ (2 vs. 3); [d,e]$P < 0.05$ (3 vs. 1); [f,g]$P < 0.05$ (4 vs. 1 and 3).
[a] Kruskal–Wallis non-parametric ANOVA.

Table 3
Micro-CT scan analysis of bone defect sites.

Group	BV (Mean ± SD)	TV (Mean ± SD)	BV/TV (%)
Untreated defect	0.34 ± 0.06	2.93 ± 0.43	11
Autograft	1.41 ± 0.44	1.48 ± 0.56	95**
G/nHAp	0.67 ± 0.05	1.83 ± 0.18	36*
CBD-PLGA-G/nHAp	1.38 ± 0.82	1.49 ± 0.66	92**

BV = bone volume (mm^3), TV = total volume (mm^3), No. of slices for evaluation = 200, slice thickness = 6 μm. *,**: indicates treatment group versus untreated group. G: gelatin, nHAp: nano hydroxyl apatite, CBD: cannabidiol, PLGA: poly (lactic-*co*-glycolic acid) microsphere.
** $P < 0.001$.
* $P < 0.01$.

dropped 500 μl of the suspension onto one side of the G/nHAp scaffold and 500 μl of the suspension onto another side of the scaffold. Finally, the microsphere-scaffold composite was lyophilized and stored at −20 °C.

2.2.4. Evaluation of porosity

We used the liquid displacement method to evaluate porosity of the fabricated scaffolds [25]. Briefly, the porous scaffolds were immersed in a graduated cylinder that had an initial volume of absolute ethanol (V1) and incubated for 5 min. The total volume of ethanol and the sample was recorded as V2. V3 was defined as the residual level of absolute ethanol after removal of the scaffold. We calculated the porosity of the scaffolds according to the following equation:

$$P\% = \frac{(V_1 - V_3)}{(V_2 - V_3)} \times 100$$

Each scaffold was analyzed in triplicate.

2.2.5. Biodegradation analysis

Biodegradability of the G/nHAp scaffold was determined according to a previously described protocol [26]. Briefly, the scaffolds (1.5 × 1.5 cm) were immersed in a simulated body fluid (SBF) solution of 0.2 ml of SBF/mm^3 of the scaffold at 37 °C. We removed the samples from the SBF at different time points (3, 7, 14, 21, and 28 days) and washed them with DW. All samples were freeze-dried and analyzed for changes in morphology and weight loss. We calculated the biodegradation rate of the G/nHAp scaffold according to the following equation:

$$D\% = \left[\frac{D_1 - D_2}{D_1} \right] \times 100$$

where, D1 was the original scaffold weight and D2 represented the weight of the freeze-dried sample after its removal from SBF. We analyzed 3 independent samples for each group.

2.2.6. Mechanical analysis of the fabricated scaffold

The compressive strength and modulus of the composites were measured at room temperature. We tested the specimen (cylindrical disk: 6 mm thickness × 12 mm diameter) with a universal tensile machine (Santam, IRI) at a crosshead speed of 1 mm/min with a 1000 N load cell.

2.2.7. Scanning electron microscopy (SEM)

We used a scanning electron microscope (Crossbeam®, 1540XB by Zeiss) to examine the surface and internal 3D architecture of the fabricated scaffolds. Pore sizes were measured in a minimum of 100 pores per scaffold. We used scanning electron microscopy (SEM) to determine the mean particle size and microsphere distribution on the scaffold.

2.2.8. In vitro release of CBD from the PLGA microspheres and CBD-PLGA-G/nHAp

We prepared a suspension of microspheres with a final concentration of 1 mg/ml in phosphate buffer saline (PBS, pH 7.4), which was subsequently incubated at 37 °C under constant agitation at 50 rpm. The released medium was entirely withdrawn at pre-determined time points followed by the addition of fresh PBS. The release of CBD from the CBD-PLGA-G/nHAp scaffold was carried out by immersing the scaffolds in PBS at 37 °C. The release medium was collected at the same time points as the microspheres. The concentration of CBD in the supernatants was determined by fluorescence spectroscopy at an excitation wavelength of 280 nm and an emission wavelength of 307 nm. The release profile was determined based on the following equation:

$$\text{Released drug}(\%) = \left[\frac{m_t}{m_0} \right] \times 100$$

where, m_t was the mass of released CBD at each time interval and m_0 was the total mass of CBD in the microspheres. The total drug content of microspheres was measured by dissolving the desired amount of microspheres in dichloromethane followed by extraction of CBD with an equal volume of water. The encapsulation efficiency was calculated based on the following equation:

$$\text{Encapsulation efficiency }(\%) = \left[\frac{m_m}{m_f} \right] \times 100$$

where, m_m was the measured mass of drug in microspheres and m_f was the mass of drug consumed for fabrication of the microspheres.

2.2.9. Quantitative RT-PCR (qRT-PCR) analysis

We seeded the MSCs onto the scaffolds and allowed to incubate for 21 days. Total RNAwas extracted from the cells using the RNeasy Micro Kit (Qiagen, 74004). cDNA was synthesized by using the Revert Aid First Strand cDNA Synthesis Kit (Fermentas, Sankt Leon-Rot, Germany, k1632) according to the manufacturer's instructions. The qRT-PCR reaction was performed with the SYBR Green Master Mix (Origene, Rockville, MD, USA) using a real-time PCR system (Applied Biosystems Life Technologies, Inc., ABI StepOnePlus) and analyzed with StepOne software (Applied Biosystems, version 2.1). Relative quantification was performed by the comparative CT method ($2^{-\Delta\Delta Ct}$ method), where a number of target genes were normalized to an endogenous control (*GAPDH*) and relative to a calibrator group (control group-2D culture flask). All reactions were performed in duplicate and we collected all of the samples from 3 biological replicates. Table S1 lists the primers.
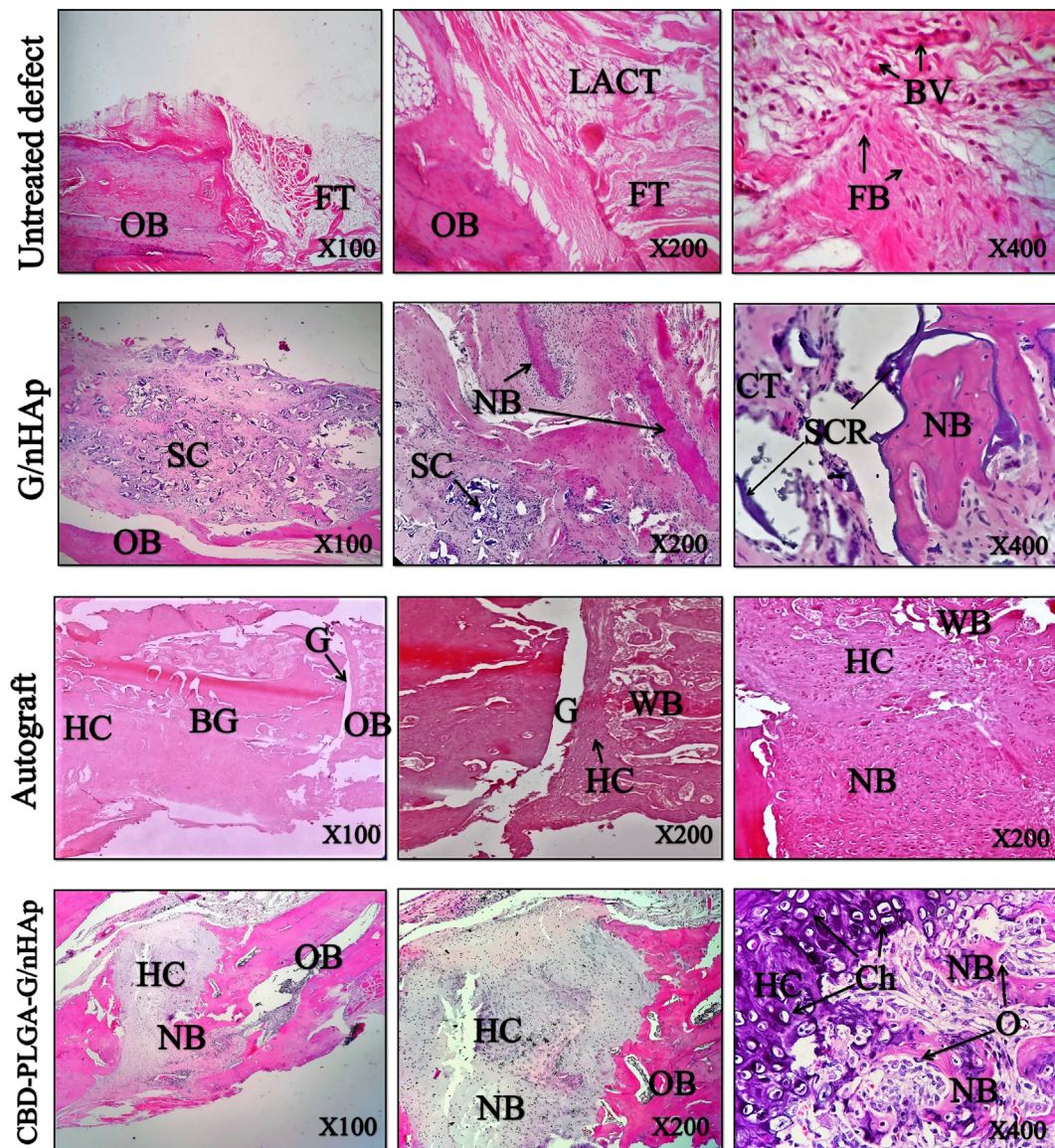
Fig. 5. Histopathological sections from the radial bone defects in rats at 4 week post-operation. There are still some remnants of the CBD-free G/nHAp scaffold, while the CBD-PLGA-G/nHAp scaffolds were completely degraded and almost replaced with new tissues including fibrous, cartilage and bone tissues. Minimum healing of the defect site was seen in the untreated defect group. LACT: loose areolar connective tissue; FT: fibrous connective tissue; OB: old bone; BM: bone marrow; BV: blood vessels, G: Gap; NB: new bone formation, BG: Bone graft, Ch: chondrocyte; HC: hyaline cartilage; WB: woven bone; SC: scaffold residue; O: osteoblast; Os: osteon, FB: fibroblast, Stained with *H&E*.

2.2.10. Animals and surgical procedures

A total of 40 adult male Wistar rats (200–250 g) were purchased from Razi Institute, Karaj, Iran. All animals were anesthetized by intramuscular (IM) injections of ketamine hydrochloride (2 mg/kg) and Xylazine (1 mg/kg). Next, we made a bilateral 3 cm incision over the rats' forearms and, subsequently, 5 mm of the radius diaphysis was ostectomized with an electrical bone saw (Strong Co., Seoul, South Korea) under normal saline irrigation. The ulnar bones were left intact as a natural protector of the defect site. The bone defects (20 defects/group) were untreated or treated with either an autograft (CBD-free G/nHAp scaffold) or CBD-PLGA-G/nHAp in the defect areas ($2 \times 2 \times 5$ mm^3) as seen in Fig. 1. The animals received 1 mg/kg meloxicam as post-operative analgesia and antibiotic therapy of 10 mg/kg enrofloxacin. This experiment was approved by the local Ethics Committee of "Regulations for using animals in scientific procedures" in the school of Veterinary Medicine, Shiraz University, Shiraz, Iran. The animals were euthanized 1, 4, and 12 week post-surgery (WPS). Their radial bones were harvested and used for subsequent experiments.

2.2.11. Gross morphology

We performed macroscopic evaluation for the presence of regeneration of the radial bone defects in each group. The results were blindly scored, as follows: 0 (non-union defects without instability), +1 (incomplete union with presence of fibrous connective tissue within the defect), +2 (incomplete union with presence of cartilage within the defect), and +3 (complete union with presence of the bridging bone) [27].

2.2.12. Radiological evaluation

Plain lateral X-rays (35 kV, 1.5 mA for 3 s) were taken of each radial bone at 4 and 12 WPS. Each radiograph was scored according to a previously described scoring system to evaluate the healing process of the radial bone defect [28].

2.2.13. Micro-computed tomography (micro-CT)

The harvested radial bone samples were assessed by a Scanco micro-CT 35 scanner (Scanco, Wangen-Brüttisellen, Switzerland) at 70 kVP,
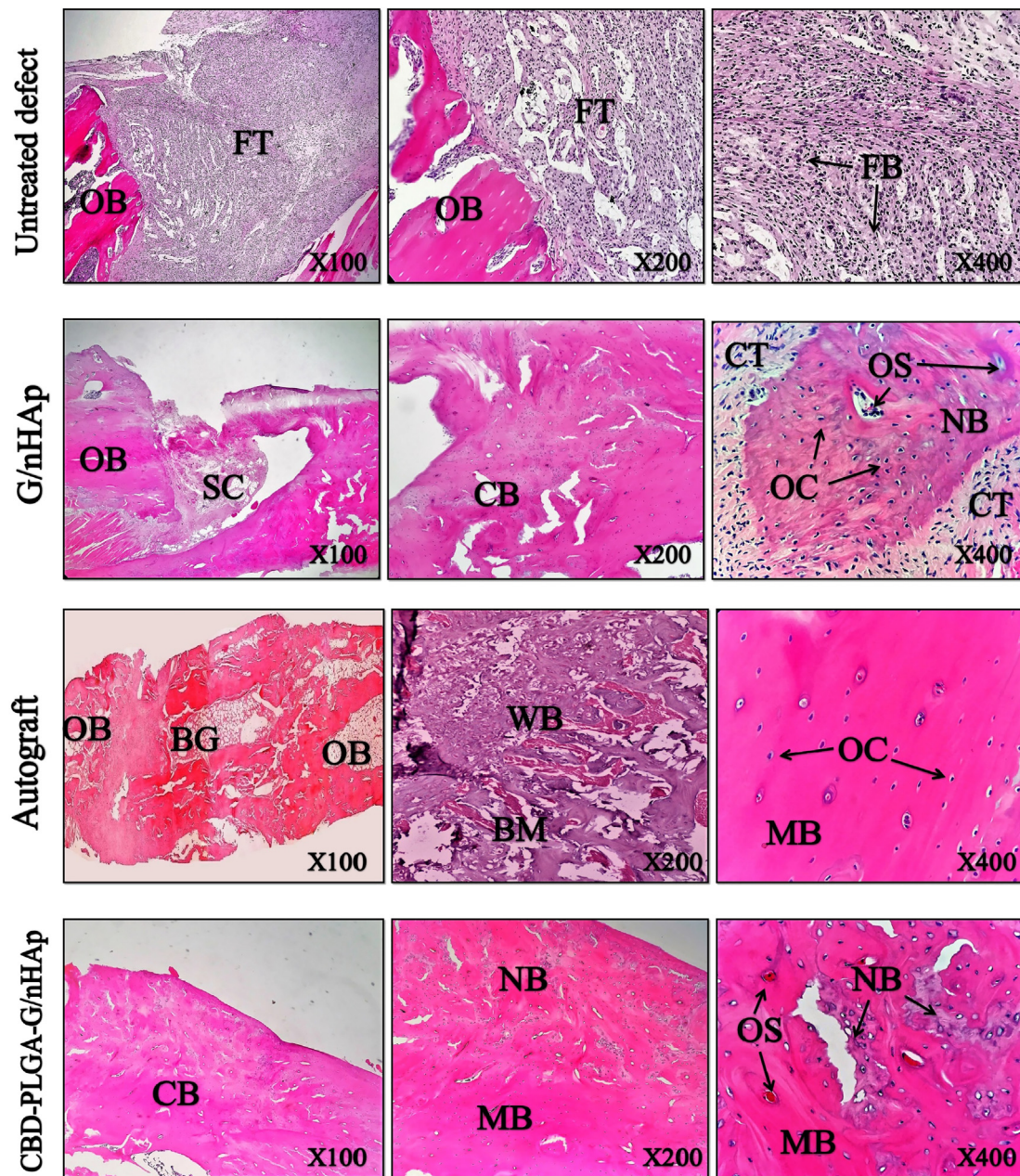
Fig. 6. Histopathological sections from the radial bone defects in rats 12 week post-operation. The CBD-free G/nHAp was degraded over time and replaced by new tissues (fibrous connective tissue, cartilage, and osseous tissue). The maximum similarity to the autograft was seen in the CBD-PLGA-G/nHAp group, in which the defect site was completely filled with new bone and cartilage tissue. FT: fibrous connective tissue; OB: old bone; BM: bone marrow; NB: new bone formation, BG: Bone graft, CT: connective tissue; OC: osteocyte; HC: hyaline cartilage; CB: compact bone; MB: mature bone, SC: scaffold residue; Os: osteon, Stained with *H&E*.

114 µA for 800 ms. We calculated bone volume (BV), total volume (TV), and the BV/TV ratio (%) based on the data obtained from the micro-CT scans.

2.2.14. Histopathologic and histomorphometric studies

The bone tissues from all groups were fixed in 10% neutral buffered formalin (NBF) solution for 48 h and then decalcified with 14% EDTA (pH 7.4) for 28 days. The decalcified bone samples were subsequently embedded in paraffin and cut into 5 µm sections. Then, they were stained with hematoxylin and eosin (H&E). The histological sections were examined by a light microscope (Olympus BX51; Olympus, Tokyo, Japan) and Evaluated by an independent pathologist who was blinded to the study groups.

2.2.15. Immunohistochemistry (IHC) analysis

IHC was performed to detect osteogenic and angiogenic differentiation of the recruited cells at the defect site (12 WPS). Histological slides were incubated with citrate buffer (Dako, Glostrup, Denmark) at 60 °C for heat-induced epitope retrieval and blocked with 1% hydrogen peroxide/methanol (Sigma-Aldrich, St Louis, MO, USA) for 30 min at room temperature. Subsequently, they were incubated overnight at 4 °C with primary antibodies OCN (ab13420, Abcam, MA, USA), OPN (ab8448, Abcam, MA, USA), and collagen type I (ColI, sc-59772, Santa Cruz Biotechnology, CA, USA). The color reaction was developed with ready-to-use 3,3′-diaminobenzidine (Dako Liquid DAB) color solution. The slides were counterstained with hematoxylin and visualized by a light microscope (Olympus BX51; Olympus, Tokyo, Japan).

We evaluated the migration of MSCs into the defect area. We did Immunofluorescence labeling of the bone sections (1 WPS) overnight at

Table 4
Histomorphometric results of the defect sites 12 week post-surgery.

Value	Untreated defect (1) (Mean ± SD)	Autograft (2) (Mean ± SD)	G/nHAp (3) (Mean ± SD)	CBD-PLGA-G/nHAp (4) (Mean ± SD)	P^a
Fibrocyte + fibroblast[b]	165.1 ± 44.2	7.5 ± 1.5	54.4 ± 5.4	9.4 ± 2.3	0.002
Chondroblast + chondrocyte[c]	3.1 ± 0.7	18.2 ± 4.8	35.4 ± 6.9	13.5 ± 2.6	0.001
Osteoblast + osteocyte[d]	5.2 ± 1.6	171.3 ± 15.5	58.1 ± 7.3	184.8 ± 17.6	0.000
Osteoclast[e]	0.00	4.4 ± 1.2	1.3 ± 0.5	3.1 ± 1.7	0.001
Blood vessels[f]	22.4 ± 8.1	7.3 ± 2.9	16.8 ± 5.2	9.4 ± 2.6	0.000
Osteon[g]	0.00	11.7 ± 2.5	1.3 ± 0.9	8.6 ± 1.5	0.001

G: gelatin, nHAp: nano hydroxyl apatite, CBD: cannabidiol, PLGA: poly (lactic-*co*-glycolic acid) microsphere.

[a] One-way ANOVA followed by Tukey post-hoc test.

[b] $P < 0.01$ (1 vs. 2 and 4); $P < 0.05$ (3 vs. 2 and 4), (1 vs. 3).

[c] $P < 0.01$ (1 vs. 2, 3 and 4); $P < 0.05$ (3 vs. 2 and 4).

[d] $P < 0.01$ (1 vs. 2 and 4); $P < 0.05$ (3 vs. 2 and 4), (1 vs. 3).

[e] $P < 0.05$ (3 vs. 2 and 4), (1 vs. and 2, 3 and 4).

[f] $P < 0.01$ (1 vs. 2 and 4); $P < 0.05$ (3 vs. 2 and 4), (1 vs. 3).

[g] $P < 0.05$ (3 vs. 2 and 4), (1 vs. and 2, 3 and 4).

4 °C with rat CD90 (ab225, Abcam) and CD29 (NBP2-16974, Novus Biologicals, San Diego, CA, USA) antibodies. After 3 washes with PBS, the sections were incubated with donkey anti-mouse AlexaFluor 488 (Abcam) and goat anti-mouse FITC (Abcam) secondary antibodies for 1 h at room temperature. The labeled sections were then washed and mounted with 100 mM glycine in PBS. The sections were imaged on a fluorescence microscope (Olympus BX51; Olympus, Tokyo, Japan).

2.2.16. Statistical analysis

The quantitative data were analyzed by one-way ANOVA with subsequent Tukey post-hoc tests. Non-parametric ANOVA and the Kruskal-Wallis test were used for statistical analysis of the qualitative data obtained from the scored values. If the differences were significant ($P < 0.05$), then the data were analyzed by the Mann-Whitney U test. All statistical analyses were assessed with GraphPad Prism software, version 6.00 (Graphpad Prism, Inc., San Diego, CA, USA).

3. Results

3.1. Characterization of the scaffolds and CBD-PLGA microsphere

SEM micrographs of the CBD-free G/nHAp revealed proper interconnectivity and large-sized pores in all fabricated scaffolds (Fig. 2A). The CBD-free G/nHAp and CBD-PLGA-G/nHAp scaffolds showed the porosity of 85.3 ± 3.4% and 89.5 ± 2.1%, respectively. The mean pore size for CBD-free G/nHAp and CBD-PLGA-G/nHAp was 345.3 ± 9.8 μm and 353 ± 7.2 μm. XRD SEM patterns of the G/nHAp scaffold showed that the angles of diffraction peaks for the Ca-P groups were similar to HA. Analysis of the XRD patterns revealed the presence of crystalline phases consistent with phases listed in the ICDD database (Fig. S1).

The presence of CBD in the PLGA microspheres was confirmed by fluorescence microscopy (Fig. S2). The PLGA microspheres did not emit fluorescence; however, the CBD-PLGA had a sharp fluorescence intensity. Fig. 2B and C show SEM micrographs of the CBD-PLGA microspheres and their distribution within the G/nHAp scaffold, respectively. The microsphere surfaces were quite smooth with no observed pores. The microspheres had a mean size of 11.6 ± 1.3 μm. The CBD-PLGA microspheres were uniformly distributed in the porous scaffold and had infiltrated into the scaffold (Fig. S3). There were no significant differences observed in the microspheres before and after incorporation into the scaffold.

We immersed the G/nHAp scaffold in SBF solution at different time points to evaluate the biodegradation rates as percent of scaffold (Fig. 3A). The rates at different time points were: 4.4 ± 1.7% (3 days), 7.2 ± 0.8% (7 days), 18.6 ± 3.2% (14 days), 26.5 ± 2.4% (21 days), and 30.7 ± 3.1% (28 days).

Fig. S4 shows the mechanical strength of the fabricated scaffolds. The compressive modulus results for the scaffolds were: 1.98 ± 0.06 (CBD-free G/nHAp) and 2.17 ± 0.48 (CBD-PLGA-G/nHAp).

3.2. Cell viability assay

Isolated cells were characterized to cofirm their mesenchymal phentotype (Fig. S5). We conducted the MTT assay at 1, 3, and 7 days to confirm MSC viability in the presence of different concentrations of CBD (Fig. S6). Based on the MTT results, we did not find any changes in cell viability in the presence of different concentrations of CBD.

3.3. In vitro release of CBD

Fig. 3B shows the in vitro release profile of CBD from the PLGA microspheres and CBD-PLGA-G/nHAp scaffold over 25 days. The encapsulation efficiency of CBD in the microspheres was 70.12 ± 4.46%. The cumulative release profile showed a continuous release of CBD from both the PLGA microspheres and CBD-PLGA-G/nHAp scaffold. However, there was a burst release during the first 48 h from the PLGA microspheres while the CBD release rate was considerably reduced by incorporation into the scaffold ($P < 0.05$). By 25 days, 71.25 ± 3.28% of the total CBD was released from the PLGA microspheres. After 25 days, 44.37 ± 4.15% of the CBD was released from the scaffolds.

3.4. qRT-PCR analysis

We used RT-PCR analysis to assess the level of osteogenic-related genes expressed by the MSCs seeded onto the fabricated scaffolds (CBD-free G/nHAp, CBD-PLGA-G/nHAp) after 21 days (Fig. 3C). CBD-PLGA-G/nHAp showed a higher expression level of *OCN* compared to the CBD-free G/nHAp and control (2D cell culture) groups ($P < 0.05$). MSCs cultured in the CBD-free G/nHAp expressed a higher level of ALP compared to the other groups ($P < 0.01$). ColI had more expression in the CBD-PLGA-G/nHAp scaffold followed by the CBD-free G/nHAp scaffold in comparison to the control ($P < 0.05$).

3.5. Assessment of bone formation by gross morphology, radiology, and micro-CT scan

We evaluated gross views of the harvested radial bones after 4 and 12 WPS (Fig. 4), and macroscopically scored them based on the newly formed tissues at 12 WPS (Table 1). The defects treated with the CBD-free G/nHAp group were replaced by fibrous and cartilaginous-like tissues. The CBD-PLGA-G/nHAp was completely filled with bony-like tissue, which was similar to the autograft. In contrast, the defect site in the untreated group remained either empty or only filled with fibrous
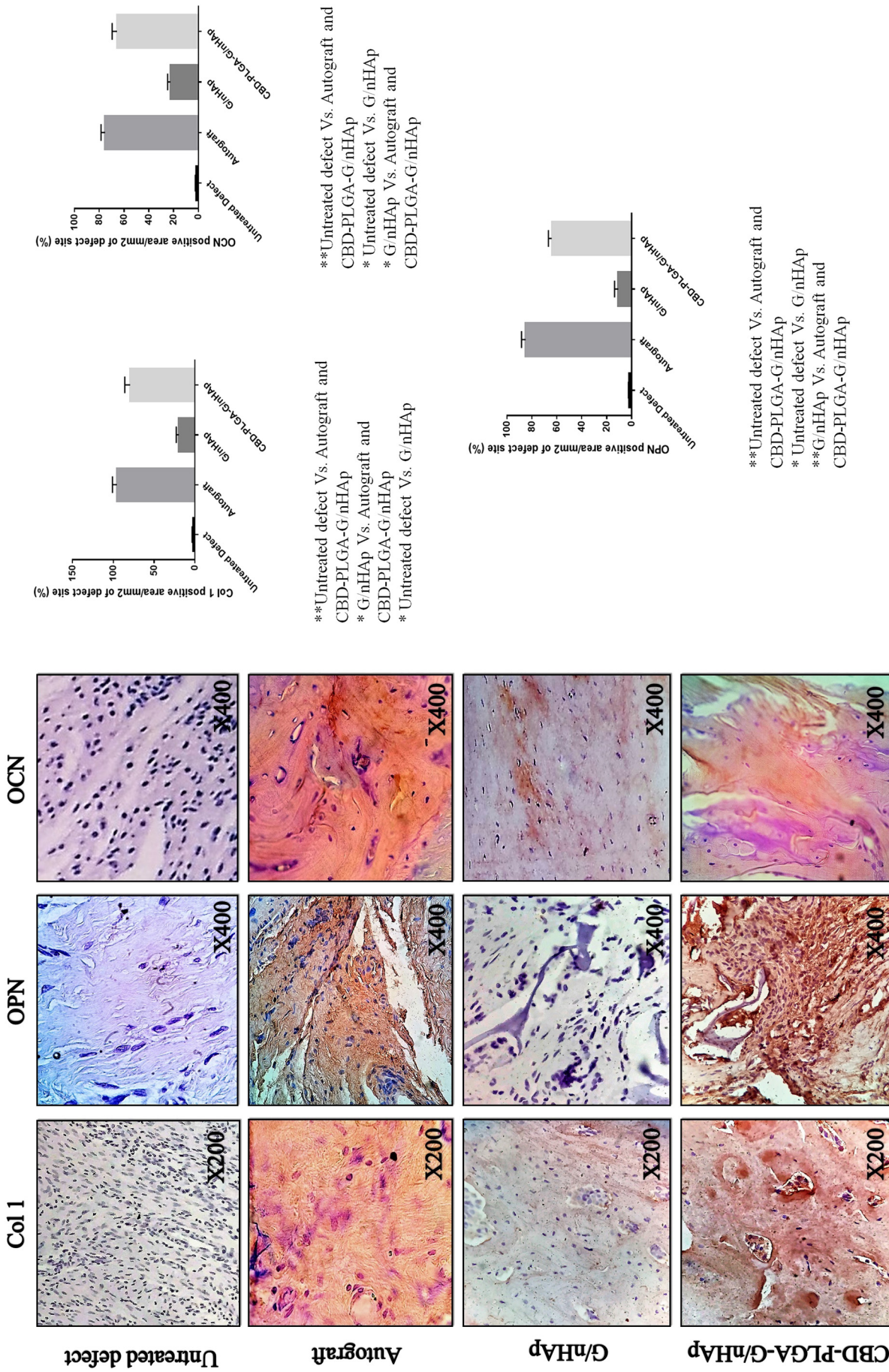
Fig. 7. Immunostaining of the injured area in different treatment groups for bone regeneration and angiogenesis. Immunohistochemical analysis of the ColI, OCN, and OPN genes was used to determine the osteogenesis and angiogenesis in the samples. The brown color represents positive staining for ColI, OCN, and OPN. **P < 0.01, *P < 0.05. (For interpretation of the references to color in this figure legend, the reader is referred to the web version of this article.)
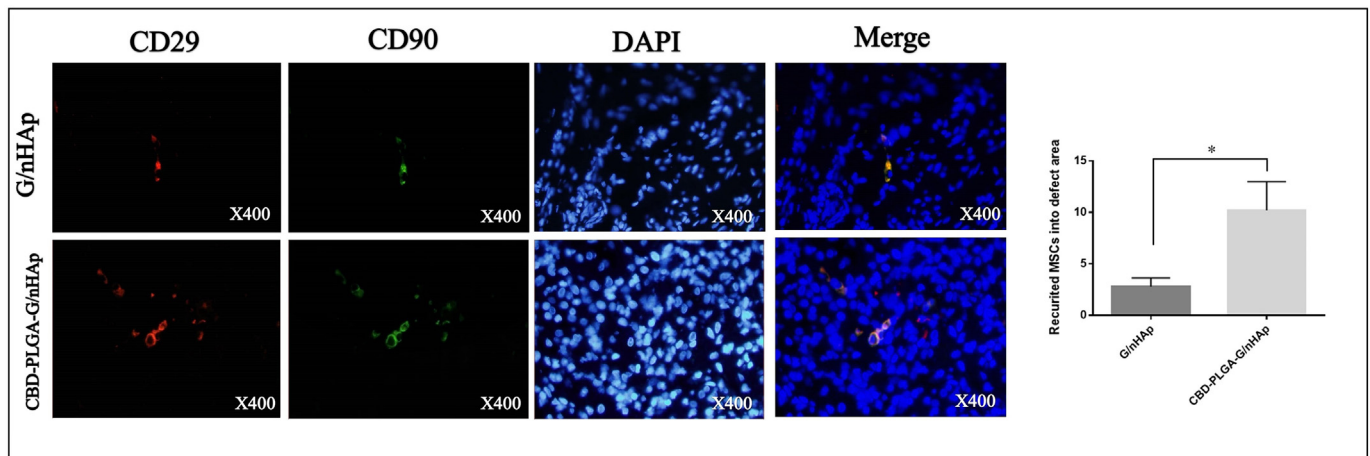
Fig. 8. Migration of the MSCs was also examined by immunostaining method. CBD treatment led to the enhanced recruitment of CD90 + /CD29 + cells to the defect site, **$P < 0.01$, *$P < 0.05$.

connective tissue. The macroscopic scores were higher in both the CBD-PLGA-G/nHAp scaffold and autograft groups compared to the CBD-free G/nHAp scaffolds ($P < 0.01$). No significant differences existed between the autograft and CBD-PLGA-G/nHAp groups in terms of macroscopic union scores ($P > 0.05$).

Fig. 4 and Table 2 show the radiographs and related scores from the experimental groups. The X-ray scores revealed superior new bone formation and unions in the CBD-PLGA-G/nHAp and autograft groups compared to the CBD-free G/nHAp scaffolds and untreated groups at 4 and 12 WPS ($P < 0.05$). We observed more significant bone union in the CBD-free G/nHAp group compared to the untreated group ($P < 0.05$). The bone gap was radiopaque in both CBD-PLGA-G/nHAp and autograft groups 12 WPS in contrast to the CBD-free G/nHAp and untreated defect, which were almost radiolucent with a range of opacities.

We conducted micro-CT scans to characterize the newly-formed tissues in the 3D images at 12 WPS (Fig. 4, Table 3). The BV/TV ratio, as an index of new bone formation, was significantly higher in the CBD-PLGA-G/nHAp (92%) and autograft (95%) groups followed by the CBD-free G/nHAp (36%) scaffold and untreated defect (11%) groups ($P < 0.05$).

3.6. Histopathologic, histomorphometric, and immunohistochemical findings

Histological analysis of the radial bones from the experimental groups was performed at 4 (Fig. 5) and 12 (Fig. 6) WPS. There was a higher degree of new bone formation and cartilaginous tissue in the CBD-PLGA-G/nHAp group, which was similar to the autograft. Histopathological analysis showed that autograft integrated to one side of the old bone after 4 weeks. Integration to both sides occurred at 12 WPS. The remnants of the CBD-free G/nHAp scaffold were present in the injury site and surrounded by fibrous connective tissue at 4 WPS. After 12 weeks, these defects were filled with fibrocartilage and cartilaginous tissues. In contrast, the bone gap was filled by a loose areolar connective tissue in the untreated group at 4 WPS, which was subsequently replaced by fibrovascular tissue at 12 WPS.

Table 4 shows histomorphometric results of newly formed osseous, cartilaginous, and fibrous tissues at 12 WPS. The osseous and cartilaginous tissues showed the highest density in the autograft and CBD-PLGA-G/nHAp groups ($P < 0.05$) followed by the CBD-free G/nHAp group. In contrast, untreated groups had significantly more dense fibrous connective tissues and immature granulation tissues (number of fibrocytes, fibroblasts, newly-formed blood vessels, and density of collagen fibers; $P < 0.01$).

We conducted IHC analysis to evaluate Col I, OCN, and OPN osteogenic related markers (Fig. 7). IHC results showed increased ColI protein expression in the autograft and CBD-PLGA-G/nHAp groups compared to the other groups ($P < 0.05$). Both OPN and OCN highly expressed in the autograft and CBD-PLGA-G/nHAp groups ($P < 0.05$). There were no OCN and OPN protein expressions detected in the untreated defect. To confirm recruitment to the defect area in response to local delivery of CBD, the bone tissue sections were stained for the MSC markers CD90 (green) and CD29 (red) as shown in Fig. 8 [27]. The 2 markers showed highly localized MSCs in the defect site. The CBD-PLGA-G/nHAp treated animals had higher numbers of MSCs compared to the CBD-free G/nHAp group.

Table S2 lists the parameters of ultimate load (N), stress (N/mm^2), strain (%) and stiffness (N/mm) obtained from the biomechanical testing. The autograft and CBD-PLGA-G/nHAp groups showed the highest ultimate load, stress, and stiffness compared to the other groups ($P < 0.01$), whereas the untreated defects showed the greatest strain ($P < 0.05$).

4. Discussion

Cannabinoids supposedly possess healing properties that are mediated through recruitment of regenerative cells into injury sites [14,29,30]. The contribution of cannabinoids in bone reconstruction and their pharmacological effects on stem cell migration is undetermined. We have selected the G/nHAp porous scaffold as an osteoconductive vehicle for local delivery of CBD to explore its bone healing potential in a preclinical setting.

Analysis of physical properties of fabricated scaffolds revealed that incorporation of CBD-PLGA in G/nHAp scaffold led to a slight change in the scaffold microstructure (i.e. porosity and pore size) which was not statistically significant. Similarly, a comparison of CBD-PLGA-G/nHAp and G/nHAp scaffolds confirmed the comparable mechanical strength in the CBD-PLGA-G/nHAp scaffold according to the compressive stress-strain curve. Here, we used post-seeding method for incorporation of CBD-PLGA into G-nHAp Scaffold. Accordingly, we expect to see no significant changes in the mechanical and structural properties of G-nHAp scaffold by using this method. These findings are in agreement with Zhang et al. study that represented incorporation of BMP2-loaded PLGA microspheres into the porous nanofibrous scaffold via post-seeding technique did not change the mechanical properties of original scaffold [31].

The in vitro release profile of CBD showed that incorporation of CBD-PLGA into the G/nHAp scaffold decreased CBD release over 25 days. Therefore, we assumed that incorporation of CBD-PLGA into

the G/nHAp scaffold controlled the CBD release in a sustainable manner. We assessed CBD biocompatibility under in vitro conditions. Based on the MTT results, different concentrations of CBD caused no significant changes in cell viability. A previous study reported that concentrations of 9 μM and greater of CBD caused significant increase in cell viability relative to the control [32]. An in vitro migration assay showed that CBD significantly induced MSC migration (Fig. S7), which was confirmed by in vivo immunostaining. Schmuhl et al. reported the effect of CBD on MSC migration at the 3 μM concentration [14], which was similar to our study (~3.2 μM). Regarding the role of cannabinoids in cellular migration, endocannabinoids such as 2-arachidonoyl glycerol and arachidonoyl cyclopropylamide were found to exert a pro-migratory impact on microglial cells via activation of "abnormal-cannabidiol-sensitive receptors" [33,34]. Another study showed that N-arachidonoyl serine (an endocannabinoid-like substance) was pro-migratory on human dermal microvascular cells [35]. These findings revealed a critical role for cannabinoids and their receptors on migration of different cell lineages.

The impact of CBD on osteogenic differentiation of MSCs was also investigated in vitro. In the current study, qRT-PCR analysis of three osteogenic markers indicated that the 21 day culture of MSCs on CBD-free G/nHAp and CBD-PLGA-G/nHAp scaffolds increased osteogenic activity of MSCs. Our findings agreed with previous studies that assessed CBD osteogenic activity [14]. The low expression of ALP in the CBD-PLGA-G/nHAp group might be related to earlier initiation of the mineralization processs. Of note, ALP is one of the earliest markers of osteoblastic cell differentiation. ALP shows a maximal expression level on day 7, which declines over time, with initiation of the mineralization process [36]. In our study, we have observed that ALP expression declined at day 21, whereas there was increased expression of the late genes, *OCN* and *COL1*. Although the CBD-free G/nHAp scaffold could trigger the differentiation of MSCs into an osteogenic lineage, this process was slower than in the CBD-PLGA-G/nHAp scaffold.

Our histopathological and histomorphometric findings combined with imaging techniques (micro-CT and radiology) showed a specific CBD-induced enhancement in new bone formation via sustained release of CBD. The CBD-PLGA-G/nHAp treated group significantly improved bone healing compared to the CBD-free G/nHAp group. In our study, the bone healing process occurred through endochondral ossification, which was mainly related to the regenerative effect of CBD. An in vivo experimental study evaluated the effect of *Cannabis sativa* (marijuana) smoke inhalation on bone healing and reported inhibition of the early stages (30 days) of bone regeneration around titanium implants [37]. Another study, in agreement with our findings, suggested the positive effects of CBD on fracture healing during the late stage of healing (after 6 weeks). These controversial results of the cannabinoids impact on bone regeneration might originate in the regeneration phase [19]. For example, peri-implant ossification is an intramembranous process. The early and reactive phases of inflammation, granulation tissue formation, and, finally its organization through primary bone formation [38], might be susceptible to the adverse effects of cannabis. Researchers have shown that the initial cartilaginous phase, which was absent in intramembranous ossification, protected the healing process from such effects [19].

Our findings showed a significantly increased BV density (BV/TV) in the defect area of the CBD-PLGA-G/nHAp scaffold compared to the CBD-free G/nHAp scaffold and untreated defects. In contrast, another study reported that CBD affected the material properties of the newly formed bone bridge based on the absence of significant differences between the CBD-treated and control animals in terms of bone mineral density [19].

The biomechanical results also showed that controlled release of CBD significantly improved the biomechanical properties of the healed bone compared to the control group. Migration of numerous MSCs and their differentiation into the osteoblastic lineage due to CBD resulted in enhanced new bone formation and improved biomechanical properties

of the defect area in this group. Another factor that might affect bone mechanical properties is the quality of the collagenous matrix. It has been shown that CBD increased expression of PLOD1, which indirectly increased the collagen crosslink ratio [19]. This ratio is an indicator of collagen maturity [39] considered extremely important for the mechanical properties of repaired bone.

Overall, the present study showed that CBD was an effective small molecule for stimulation of MSCs migration and their differentiation into osteogenic lineages, which rendered the osteoinductivity for osteoconductive (e.g., G/nHAp) scaffolds. Controlled delivery of CBD could be utilized in the future in commercial bone tissue scaffolds to increase bone healing, particularly in critical-sized bone defects. Further investigations would be required to examine the optimal CBD concentration in a controlled delivery system for bone regeneration.

5. Conclusion

We developed and evaluated of a novel scaffold for healing of large bone defects. The results indicated that this scaffold was reliable and had acceptable therapeutic efficacy. We observed migration of the BM-MSCs towards the injury site and their differentiation into osteoblasts, which indicated an appropriate biocompatibility and osteoinductivity of the fabricated scaffold. Controlled-release of CBD enhanced MSC recruitment and bone reconstruction, which were confirmed by various analyses. Based upon the in vitro and in vivo results, the CBD-PLGA-G/nHAp scaffold could be introduced as a promising alternative to conventional treatments. The results of the present study provided first-time in vivo evidence for induction of MSCs recruitment and their osteogenic differentiation by controlled local delivery of CBD.

Acknowledgment

Conflict of interest

The authors declare that they have no conflicts of interest.

Appendix A. Supplementary data

Supplementary data to this article can be found online at https://doi.org/10.1016/j.msec.2019.03.070.

References

[1] A. Oryan, S. Alidadi, A. Moshiri, N. Maffulli, Bone regenerative medicine: classic options, novel strategies, and future directions, J. Orthop. Surg. Res. 9 (2014) 18.
[2] R. Dimitriou, E. Jones, D. McGonagle, P.V. Giannoudis, Bone regeneration: current concepts and future directions, BMC Med. 9 (2011) 66.
[3] A. Oryan, A. Kamali, A. Moshiri, M. Baghaban Eslaminejad, Role of mesenchymal stem cells in bone regenerative medicine: what is the evidence? Cells Tissues Organs 204 (2017) 59–83.
[4] A. Oryan, S. Alidadi, A. Moshiri, Platelet-rich plasma for bone healing and regeneration, Expert. Opin. Biol. Ther. 16 (2016) 213–232.
[5] S. Bose, M. Roy, A. Bandyopadhyay, Recent advances in bone tissue engineering scaffolds, Trends Biotechnol. 30 (2012) 546–554.
[6] G. Despars, C.L. Carbonneau, P. Bardeau, D.L. Coutu, C.M. Beauséjour, Loss of the osteogenic differentiation potential during senescence is limited to bone progenitor cells and is dependent on p53, PLoS ONE 8 (2013) e73206.
[7] A. De Becker, I.V. Riet, Homing and migration of mesenchymal stromal cells: how to improve the efficacy of cell therapy? World J. Stem Cells 8 (2016) 73–87.
[8] X. Shen, Y. Zhang, Y. Gu, Y. Xu, Y. Liu, B. Li, L. Chen, Sequential and sustained release of SDF-1 and BMP-2 from silk fibroin-nanohydroxyapatite scaffold for the enhancement of bone regeneration, Biomaterials 106 (2016) 205–216.
[9] Q. Jin, W.V. Giannobile, SDF-1 enhances wound healing of critical-sized calvarial defects beyond self-repair capacity, PLoS One 9 (2014).
[10] H. Liu, M. Li, M. Du, P. Yang, S. Ge, Local administration of stromal cell-derived factor-1 promotes stem cell recruitment and bone regeneration in a rat periodontal

bone defect model, Mater. Sci. Eng. C Mater. Biol. Appl. 53 (2015) 83–94.

[11] M.B. Delgado, I. Clark-Lewis, P. Loetscher, H. Langen, M. Thelen, M. Baggiolini, M. Wolf, Rapid inactivation of stromal cell-derived factor-1 by cathepsin G associated with lymphocytes, Eur. J. Immunol. 31 (2001) 699–707.

[12] D.I. Bromage, S. Taferner, M. Pillai, D.M. Yellon, S.M. Davidson, A novel recombinant antibody specific to full-length stromal derived factor-1 for potential application in biomarker studies, PLoS ONE 12 (2017) e0174447.

[13] R.K. Mishra, A.K. Shum, L.C. Platanias, R.J. Miller, G.E. Schiltz, Discovery and characterization of novel small-molecule CXCR4 receptor agonists and antagonists, Sci. Rep. 6 (2016) 30155.

[14] E. Schmuhl, R. Ramer, A. Salamon, K. Peters, B. Hinz, Increase of mesenchymal stem cell migration by cannabidiol via activation of p42/44 MAPK, Biochem. Pharmacol. 87 (2014) 489–501.

[15] M.A. Huestis, Human cannabinoid pharmacokinetics, Chem. Biodivers. 4 (2007) 1770–1804.

[16] F. Grotenhermen, Pharmacology of cannabinoids, Neuro Endocrinol. Lett. 25 (2004) 14–23.

[17] O. Devinsky, J.H. Cross, L. Laux, E. Marsh, I. Miller, R. Nabbout, I.E. Scheffer, E.A. Thiele, S. Wright, Trial of cannabidiol for drug-resistant seizures in the Dravet syndrome, N. Engl. J. Med. 376 (2017) 2011–2020.

[18] C. Ridler, Epilepsy: cannabidiol reduces seizure frequency in Dravet syndrome, Nat. Rev. Neurol. 13 (2017) 383–383.

[19] N.M. Kogan, E. Melamed, E. Wasserman, B. Raphael, A. Breuer, K.S. Stok, R. Sondergaard, A.V. Escudero, S. Baraghithy, M. Attar-Namdar, S. Friedlander-Barenboim, N. Mathavan, H. Isaksson, R. Mechoulam, R. Muller, A. Bajayo, Y. Gabet, I. Bab, Cannabidiol, a major non-psychotropic cannabis constituent enhances fracture healing and stimulates lysyl hydroxylase activity in osteoblasts, J. Bone Miner. Res. Off. J. Am. Soc. Bone Miner. Res. 30 (2015) 1905–1913.

[20] I. Bab, A. Zimmer, E. Melamed, Cannabinoids and the skeleton: from marijuana to reversal of bone loss, Ann. Med. 41 (2009) 560–567.

[21] T.S. Yu, Z.H. Cheng, L.Q. Li, R. Zhao, Y.Y. Fan, Y. Du, W.X. Ma, D.W. Guan, The cannabinoid receptor type 2 is time-dependently expressed during skeletal muscle wound healing in rats, Int. J. Legal Med. 124 (2010) 397–404.

[22] S. Kozono, T. Matsuyama, K.K. Biwasa, K. Kawahara, Y. Nakajima, T. Yoshimoto, Y. Yonamine, H. Kadomatsu, S. Tancharoen, T. Hashiguchi, K. Noguchi, I. Maruyama, Involvement of the endocannabinoid system in periodontal healing, Biochem. Biophys. Res. Commun. 394 (2010) 928–933.

[23] I. Bab, A. Zimmer, Cannabinoid receptors and the regulation of bone mass, Br. J. Pharmacol. 153 (2008) 182–188.

[24] W. Zeng, M. Rong, X. Hu, W. Xiao, F. Qi, J. Huang, Z. Luo, Incorporation of chitosan microspheres into collagen-chitosan scaffolds for the controlled release of nerve growth factor, PLoS ONE 9 (2014) e101300.

[25] A.L. Torres, V.M. Gaspar, I.R. Serra, G.S. Diogo, R. Fradique, A.P. Silva, I.J. Correia, Bioactive polymeric–ceramic hybrid 3D scaffold for application in bone tissue regeneration, Mater. Sci. Eng. C 33 (2013) 4460–4469.

[26] A. Oryan, M. Baghaban Eslaminejad, A. Kamali, S. Hosseini, F.A. Sayahpour, H. Baharvand, Synergistic effect of strontium, bioactive glass and nano-

hydroxyapatite promotes bone regeneration of critical-sized radial bone defects, J Biomed Mater Res B Appl Biomater 107 (2019) 50–64.

[27] A.M. Parizi, A. Oryan, Z. Shafiei-Sarvestani, A.S. Bigham, Human platelet rich plasma plus Persian Gulf coral effects on experimental bone healing in rabbit model: radiological, histological, macroscopical and biomechanical evaluation, J. Mater. Sci. Mater. Med. 23 (2012) 473–483.

[28] A. Oryan, A. Bigham-Sadegh, F. Abbasi-Teshnizi, Effects of osteogenic medium on healing of the experimental critical bone defect in a rabbit model, Bone 63 (2014) 53–60.

[29] H. Yang, Z. Wang, J.E. Capo-Aponte, F. Zhang, Z. Pan, P.S. Reinach, Epidermal growth factor receptor transactivation by the cannabinoid receptor (CB1) and transient receptor potential vanilloid 1 (TRPV1) induces differential responses in corneal epithelial cells, Exp. Eye Res. 91 (2010) 462–471.

[30] K. Wright, N. Rooney, M. Feeney, J. Tate, D. Robertson, M. Welham, S. Ward, Differential expression of cannabinoid receptors in the human colon: cannabinoids promote epithelial wound healing, Gastroenterology 129 (2005) 437–453.

[31] Q. Zhang, M. Qin, X. Zhou, W. Nie, W. Wang, L. Li, C. He, Porous nanofibrous scaffold incorporated with S1P loaded mesoporous silica nanoparticles and BMP-2 encapsulated PLGA microspheres for enhancing angiogenesis and osteogenesis, J. Mater. Chem. B 6 (2018) 6731–6743.

[32] M. Solinas, P. Massi, A.R. Cantelmo, M.G. Cattaneo, R. Cammarota, D. Bartolini, V. Cinquina, M. Valenti, L.M. Vicentini, D.M. Noonan, A. Albini, D. Parolaro, Cannabidiol inhibits angiogenesis by multiple mechanisms, Br. J. Pharmacol. 167 (2012) 1218–1231.

[33] A. Franklin, N. Stella, Arachidonylcyclopropylamide increases microglial cell migration through cannabinoid CB2 and abnormal-cannabidiol-sensitive receptors, Eur. J. Pharmacol. 474 (2003) 195–198.

[34] J.Y. Su, A.C. Vo, 2-Arachidonylglyceryl ether and abnormal cannabidiol-induced vascular smooth muscle relaxation in rabbit pulmonary arteries via receptor-pertussis toxin sensitive G proteins-ERK1/2 signaling, Eur. J. Pharmacol. 559 (2007) 189–195.

[35] X. Zhang, Y. Maor, J.F. Wang, G. Kunos, J.E. Groopman, Endocannabinoid-like N-arachidonoyl serine is a novel pro-angiogenic mediator, Br. J. Pharmacol. 160 (2010) 1583–1594.

[36] M.H. Choi, W.C. Noh, J.W. Park, J.M. Lee, J.Y. Suh, Gene expression pattern during osteogenic differentiation of human periodontal ligament cells in vitro, J. Periodontal Implant Sci. 41 (2011) 167–175.

[37] R. Nogueira-Filho Gda, T. Cadide, B.T. Rosa, T.G. Neiva, R. Tunes, D. Peruzzo, F.H. Nociti, Jr, J.B. Cesar-Neto, Cannabis sativa smoke inhalation decreases bone filling around titanium implants: a histomorphometric study in rats, Implant. Dent., 17 (2008) 461–470.

[38] D. Kohavi, Bone reaction to implants, in: J.J. Sela, I.A. Bab (Eds.), Principles of Bone Regeneration, Springer US, Boston, MA, 2012, pp. 119–126.

[39] E.P. Paschalis, K. Verdelis, S.B. Doty, A.L. Boskey, R. Mendelsohn, M. Yamauchi, Spectroscopic characterization of collagen cross-links in bone, J. Bone Miner. Res. Off. J. Am. Soc. Bone Miner. Res. 16 (2001) 1821–1828.